

Critical Behavior of Electrical Transport in Sea Ice

K. M. Golden^{1*}, H. Eicken², A. Gully¹, M. Ingham³,
K. A. Jones³, J. Lin¹, J. Reid⁴, C. Sampson¹ and A. P. Worby⁵

¹University of Utah, Department of Mathematics
155 S 1400 E RM 233, Salt Lake City, UT 84112-0090 USA

²Geophysical Institute, P.O. Box 757320
University of Alaska, Fairbanks, AK 99775-7320, USA

³School of Chemical and Physical Sciences, Victoria University of Wellington
P.O. Box 600, Wellington, New Zealand

⁴Geoforce Pty. Ltd., 288 Victoria Rd, Perth, 6090, Australia

⁵Australian Antarctic Division and ACE CRC,
University of Tasmania, Private Bag 80, Hobart, 7001, Australia

*To whom correspondence should be addressed; E-mail: golden@math.utah.edu

Fluid transport through porous sea ice mediates a broad range of geophysical and biological processes, such as melt pond evolution and nutrient replenishment for microbial communities. However, fluid can flow through columnar sea ice only if the brine volume fraction is above about 5%. In two very different experiments conducted in the Arctic and Antarctic, we have found the electrical signature of this *on-off* switch for fluid flow. Conductivity data from both poles is accurately explained by percolation theory with a universal critical exponent. The data also indicate marked changes in the conductivity profile with the onset of melt ponds. Our findings lay the foundation for the use of electromagnetic monitoring of transport phenomena which must be better understood to improve projections of the fate of the polar ice packs and their ecosystems.

The polar sea ice packs form a key component of Earth’s climate system, and are leading indicators of climate change (1,2). They also host extensive algal and bacterial communities which sustain life in the polar oceans (1,3). While global climate models predict declines in sea ice extent, they have significantly underestimated the dramatic losses observed in the Arctic (4). On the other hand, Antarctic sea ice has increased, along with some significant regional losses (5).

Improving projections of the fate of Earth’s ice packs and their complex ecosystems depends on a better understanding of key processes and feedback mechanisms. For example, the evolution of melt ponds and summer ice albedo is constrained by drainage through porous sea ice (6). It is believed that ice-albedo feedback has played a key role in the decline of summer Arctic sea ice (7). Fluid flow through sea ice mediates the evolution of salinity profiles (1), convection-enhanced thermal transport (8), ocean-ice-atmosphere CO₂ exchanges (9), and biomass build-up fueled by nutrient fluxes (1,3). It also enables snow-ice formation, where sea water floods the ice surface and then freezes, accounting for more than a quarter of the ice produced in the Southern Ocean (10).

It has been observed that for brine volume fractions ϕ below about 5%, columnar sea ice is effectively impermeable to vertical fluid flow, yet is increasingly permeable for ϕ above 5% (11). For a typical bulk salinity of 5 ppt, the critical porosity $\phi_c \approx 5\%$ corresponds to a temperature $T_c \approx -5^\circ$ C, which is known as the *rule of fives*. This critical behavior of the fluid permeability, which constrains the above processes, reflects a connectivity or percolation threshold in the brine microstructure (11–13). If the fluid transport properties of sea ice can be quantitatively connected to its electrical properties, which is directly addressed here, then a new class of techniques can be brought to bear in monitoring sea ice. For example, it could open the door to the development of easily deployed, expendable sensors providing information that could be integrated with satellite data.

The electrical conductivity of sea ice has been studied over the past five decades (14–19).

Success in relating the electrical transport properties to microstructural characteristics of sea ice, however, has been somewhat limited. In particular, there have been no observations of critical behavior in electrical properties corresponding to the important microstructural transition expressed by the rule of fives. Here we report on two types of experiments conducted on sea ice in the polar regions. In both cases we have obtained extensive data on the electrical resistivity which clearly display critical behavior at the brine percolation threshold. Our mathematical description provides a rigorous link between fluid and electrical transport in sea ice, with both properties displaying the same type of universal critical behavior, thus laying the foundation for the types of techniques described above.

In the Antarctic, we have made the first *direct* measurements of the vertical resistivity of sea ice using a four probe Wenner array on extracted ice cores. In the Arctic, we have used the emerging technique of cross-borehole DC tomography, utilizing four vertical strings of electrodes frozen into the ice (19,20). The vertical component of the resistivity is obtained indirectly from tomographic reconstructions of the horizontal and geometric mean resistivities. Although the two data sets were obtained at opposite ends of the Earth and by quite different methods, they agree closely and are both accurately captured with the same critical exponent from lattice percolation theory used to predict fluid permeability (12). Moreover, the Arctic data was taken in late spring and exhibits temporal behavior which is closely correlated with the onset of melt ponds.

The findings presented here also have implications for measuring ice thickness, an important gauge of the impact of global warming. Not only is thickness data important in comparing climate model predictions to observed behavior, but in specifying the initial conditions necessary for long-term numerical simulations. Almost all methods for obtaining such data depend on the interaction of electromagnetic (EM) fields with sea ice. For example, there has been significant interest in the development of EM induction devices (18,21) mounted on ships, planes and helicopters. These techniques, and the interpretation of the

data to obtain thickness information, rely on knowledge of the electrical properties of sea ice, and how they vary with depth, temperature, salinity, and ice type. The results presented here shed significant light on such issues.

During the Sea Ice Physics and Ecosystem Experiment (SIPEX) in September and October of 2007, we measured the electrical conductivity of first year Antarctic pack ice. The study area was located off the coast of East Antarctica, between 115° E and 130° E, and 64° S and 66° S. Traditional surface-based geophysical techniques for *in situ* measurement of resistivity structure, such as the Wenner array used for surface impedance tomography, have been of limited utility, particularly in relating electrical response to microstructural characteristics (14, 16, 17, 19, 22). During SIPEX we adapted the Wenner array to directly measure the vertical component of the anisotropic conductivity tensor σ^* of sea ice. At 8 of the 15 ice stations along the cruise track of the Australian icebreaker *Aurora Australis*, we used a Wenner electrode array along sections of extracted ice cores. The array was connected to a YEW Earth Resistance Tester operating at 38 Hz. As indicated in Figure 1 (A) and (B), this set-up yields the resistance along the axis of the cylindrical ice core between probes P1 and P2, corresponding to the vertical direction *in situ*. We obtained 26 averaged data points from 67 raw measurements. Temperature and salinity measurements allowed us to calculate a brine volume fraction profile for each core (1).

Through numerical simulations, we have shown that for the probe spacings and ice core geometry used here, the difference in measurements between the four probe array and a more standard parallel plate configuration is less than 1.5%. These findings establish the Wenner array as a viable field method for *direct* resistivity measurements.

The technique of cross-borehole DC resistivity tomography (19), where ice is probed in its natural state, utilizes vertical strings of electrodes frozen into the ice. It has been shown that this method can be used to derive the horizontal component of the anisotropic resistivity profile. Moreover, it has recently been demonstrated that the vertical component

of σ^* can be obtained as well (19, 20). If a minimum of four electrode strings are used, as shown in Figure 1 (C), the geometric mean of the vertical and horizontal components of σ^* can be derived, along with the horizontal component (19), yielding the vertical component.

Measurements of the temporal variation in the resistivity structure of first year Arctic sea ice through spring warming have been made approximately 1 km off the coast of Barrow, Alaska at $71^\circ 21' 56.45''$ N, $156^\circ 32' 39.01''$ W. Electrode strings were installed in landfast first year ice in late January 2008. Cross-borehole measurements were made on 6 separate occasions between early April and mid June 2008, allowing both the horizontal and vertical components of the ice resistivity to be derived. A sea ice mass balance site operated by the University of Alaska Fairbanks at the same location (23) provided ice temperature and salinity data, allowing the variation in resistivity structure to be correlated with brine volume fraction ϕ .

Lattice and continuum percolation theories (24) have been used to model a broad range of disordered materials where the connectedness of one phase dominates effective behavior. Consider the square ($d = 2$) or cubic ($d = 3$) network of bonds joining nearest neighbor sites on the integer lattice \mathbb{Z}^d . The bonds are assigned electrical conductivities $\sigma_0 > 0$ (open) or 0 (closed) with probabilities p and $1 - p$. Groups of connected open bonds are called open clusters, and the average cluster size grows as p increases. In this model there is a critical probability p_c , $0 < p_c < 1$, called the *percolation threshold*, where an infinite cluster of open bonds first appears. In $d = 2$, $p_c = \frac{1}{2}$, and in $d = 3$, $p_c \approx 0.25$. Typical configurations for the $d = 2$ square lattice above and below the threshold are shown in Figure 2.

Let $\sigma^*(p)$ be the effective conductivity of this random resistor network in the vertical direction (24). For $p < p_c$, $\sigma^*(p) = 0$, as shown in Figure 2 (C). For $p > p_c$ near the threshold, $\sigma^*(p)$ exhibits power law behavior,

$$\sigma^*(p) \sim \sigma_0(p - p_c)^t, \quad p \rightarrow p_c^+, \quad (1)$$

where t is the conductivity critical exponent. For lattices, t is believed to be universal, depending only on d . In $d = 2$, $t \approx 1.3$, and in $d = 3$, $t \approx 2.0$ (24). There is also a rigorous bound (25) that $1 \leq t \leq 2$ in $d = 2$ and $d = 3$. Since $\sigma^*(p) \rightarrow 0$ as $p \rightarrow p_c^+$, the effective resistivity $\rho^*(p) = 1/\sigma^*(p)$ diverges as $p \rightarrow p_c^+$, with a vertical asymptote at $p = p_c$, as shown in Figure 2 (D). The fluid permeability $\kappa^*(p)$ corresponding to (1), where the open bonds are pipes of fluid conductivity $\kappa_0/\eta = r_0^2/8\eta$ and radius r_0 , behaves like $\kappa^*(p) \sim \kappa_0(p - p_c)^e$ as $p \rightarrow p_c^+$, with e the fluid permeability exponent and η the fluid viscosity. For lattices, it is believed that $e = t$ (24). In the continuum, the permeability and conductivity exponents e and t can take non-universal values, and need not be equal, such as for the three dimensional Swiss cheese model (24, 26). However, for lognormally distributed inclusions, as in sea ice, the behavior is *universal* (12, 27). Thus for sea ice, $t = e \approx 2$.

In order to use percolation theory to quantitatively describe the vertical conductivity $\sigma_v^*(\phi)$, and to provide the first link between fluid and electrical transport in sea ice, we recall our result for the vertical fluid permeability $k_v^*(\phi)$ (12),

$$k_v^*(\phi) \sim 3 (\phi - \phi_c)^2 \times 10^{-8} \text{ m}^2, \quad \phi \rightarrow \phi_c^+. \quad (2)$$

The scaling factor $k_0 = 3 \times 10^{-8}$ is estimated using critical path analysis (24, 28). The effective behavior of media with a broad range of local conductances is dominated by a critical *bottleneck* conductance related to the minimal radius in a connected pathway of appropriate scale. To relate σ_v^* to k_v^* , we use the following relation from critical path analysis (28). With r_c denoting the critical radius for our centimeter scale electrical experiments, then

$$k_v^* = \frac{r_c^2}{8} \frac{\sigma_v^*}{\sigma_b}, \quad (3)$$

where σ_b is the conductivity of brine, which depends on temperature T (29). By measuring the radii of vertical pathways in X-ray tomography images (12, 13), we estimate r_c (mm) to be in the range $0.1 \leq r_c \leq 0.2$.

It is useful to consider the vertical conductivity formation factor $F = \sigma_v^*/\sigma_b$, which removes the dependence of the effective parameter on the changing conductivity of the brine, and depends only on the pore volume fraction and geometry. In view of (1) and (3), $F(\phi) \sim F_0 (\phi - \phi_c)^2$ as $\phi \rightarrow \phi_c^+$, where $F_0 = 8k_0/r_c^2$. The estimates for r_c yield a range for F_0 of $6 \leq F_0 \leq 24$.

In order to compare our conductivity measurements with percolation theory, we must exclude data below $\phi_c \approx 0.05$, as in (12), since the theory is only valid for $\phi > \phi_c$. It is more illustrative to display the data in terms of the reciprocal $1/F = \rho_v^*/\rho_b$, which is the vertical resistivity formation factor. In Figure 2 (E) we show the two data sets from the Arctic and Antarctic. By fixing the exponent $t = 2$ and the threshold value $\phi_c = 0.05$ in the above expression for $F(\phi)$, a statistical best fit of the data yields a value of $F_0 \approx 9$, which lies inside our predicted range, so that

$$F(\phi) \sim 9 (\phi - 0.05)^2, \quad \phi \rightarrow \phi_c^+. \quad (4)$$

We see that the data agree well with the theory, and that they both exhibit divergent behavior with a vertical asymptote at the percolation threshold. Moreover, in Figure 2 (F) the Antarctic data is displayed in the logarithmic variables $x = \log(\phi - 0.05)$ and $y = \log F$. The line predicted by percolation theory in (4) is $y = 2x + \log F_0$, with $\log F_0 = 0.95$, $F_0 = 9$. Critical path analysis yields the bounds $0.8 \leq \log F_0 \leq 1.4$, and the statistical best fit for the Antarctic data in (F) is $y = 1.99x + 0.93$, where 0.93 lies inside these bounds.

To model $\sigma_v^*(\phi)$ over all porosities, we consider features of the brine phase present over the full range – some degree of small-scale connectivity, and self-similarity. Hierarchical models of spheres or other grains surrounded by smaller spheres, and so on, with brine in the pore spaces, were used to model $k_v^*(\phi)$ in (12). The simplest model yields a result of $k_v^*(\phi) = k_0 \phi^3$. Via (3) we obtain an Archie's law result of $F(\phi) = F_0 \phi^3$. A statistical best fit of our Antarctic data yields a value of $F_0 \approx 16$, which is again in the estimated range.

In Figure 3 (A), our Antarctic conductivity data is shown along with both theories, and in (B), Arctic permeability data (12) is shown with both theories.

Finally, in Figure 4 we show cross-borehole tomographic reconstructions of the vertical resistivity formation factor for Arctic sea ice. In (A), the profile was obtained before the onset of melt pond formation. The ice is cold and electrically resistive. In (B), the profile was obtained well after a melt pond had formed. The ice is warmer and significantly more conductive. By 16-17 June the ice had not only thinned but had obliterated from the surface. The top 2 electrodes in each string were in air, and the third was in meltwater, so that the top 0.3 m of the profile are blank. Further, the very high resistivity in the next 0.1-0.2 m likely results from the fact that in this region fresh meltwater had percolated downwards, replacing the brine. This leads to values of the resistivity in this top layer of the ice roughly two to three times higher than before the formation of the meltpond. In the bottom 0.1 m or so, we also see highly conductive ice, likely due to high porosity and sea water infiltration.

It has been demonstrated in field experiments conducted in both the Arctic and Antarctic that sea ice exhibits critical behavior in its electrical transport properties at a percolation threshold. Such behavior provides the electrical signature of a key transition in fluid transport properties, known as the “rule of fives,” which determines whether or not fluid can flow through sea ice. This *on–off* switch for fluid flow constrains a broad range of processes which are important in the geophysics and biology of the polar regions. The phenomenon is explained theoretically using percolation theory, which provides a universal power law describing the data from both poles, as well as the first rigorous link between the fluid and electrical transport properties of sea ice. Our findings open the door to a new generation of techniques for *in situ* analysis and remote monitoring of transport processes which are critical to improving projections of the future trajectory of the polar ice packs.

Acknowledgements are in (30).

References and Notes

1. D. N. Thomas, G. S. Dieckmann, eds., *Sea Ice, 2nd Edition* (Wiley-Blackwell, Oxford, 2009).
2. M. C. Serreze, M. M. Holland, J. Stroeve, *Science* **315**, 1533 (2007).
3. C. H. Fritsen, V. I. Lytle, S. F. Ackley, C. W. Sullivan, *Science* **266**, 782 (1994).
4. J. Boé, A. Hall, X. Qu, *Nature Geoscience* **2**, 341 (2009).
5. J. Zhang, *J. Climate* **20**, 2515 (2007).
6. H. Eicken, T. C. Grenfell, D. K. Perovich, J. A. Richter-Menge, K. Frey, *J. Geophys. Res. (Oceans)* **109**, C08007.1 (2004).
7. D. K. Perovich, J. A. Richter-Menge, K. F. Jones, B. Light, *Geophys. Res. Lett.* **35**, L11501, doi:10.1029/2008GL034007 (2008).
8. V. I. Lytle, S. F. Ackley, *J. Geophys. Res.* **101**, 8853 (1996).
9. S. Rysgaard, J. Bendtsen, L. T. Pedersen, H. Ramløv, R. N. Glud, *J. Geophys. Res.* **114**, C09011, doi:10.1029/2008JC005088 (2009).
10. T. Maksym, T. Markus, *J. Geophys. Res.* **113**, C02S12, doi:10.1029/2006JC004085 (2008).
11. K. M. Golden, S. F. Ackley, V. I. Lytle, *Science* **282**, 2238 (1998).
12. K. M. Golden, *et al.*, *Geophys. Res. Lett.* **34**, L16501 (6 pages and issue cover), doi:10.1029/2007GL030447 (2007).
13. D. J. Pringle, J. E. Miner, H. Eicken, K. M. Golden, *J. Geophys. Res. (Oceans)* **114** (C12017) (2009).

14. K. Fujino, Y. Suzuki, *Low Temp. Sci.* **A21**, 151 (1963).
15. J. Addison, *J. Appl. Phys.* **40**, 3105 (1969).
16. F. Thyssen, H. Kohnen, M. V. Cowan, G. W. Timco, *Polarforschung* **44**, 117 (1974).
17. R. G. Buckley, M. P. Staines, W. H. Robinson, *Cold Reg. Sci. Technol.* **12**, 285 (1986).
18. J. E. Reid, A. Pfaffling, A. P. Worby, J. R. Bishop, *Ann. Glaciol.* **44**, 217 (2006).
19. M. Ingham, D. J. Pringle, H. Eicken, *Cold Reg. Sci. Technol.* **52**, 263 (2008).
20. K. A. Jones, M. Ingham, D. J. Pringle, H. Eicken, *J. Geophys. Res.*, *in press.* (2010).
21. C. Haas, *Geophys. Res. Lett.* **31**, L09402, doi:10.1029/2007GL030447 (2004).
22. C. Sampson, K. M. Golden, A. Gully, A. P. Worby, Surface impedance tomography for Antarctic sea ice (2010). Submitted to *Deep Sea Res.*
23. M. L. Druckenmiller, H. Eicken, M. A. Johnson, D. J. Pringle, C. C. Williams, *Cold Reg. Sci. Technol.* **56**, 61 (2009).
24. D. Stauffer, A. Aharony, *Introduction to Percolation Theory, Second Edition* (Taylor and Francis Ltd., London, 1992).
25. K. Golden, *Phys. Rev. Lett.* **65**, 2923 (1990).
26. B. I. Halperin, S. Feng, P. N. Sen, *Phys. Rev. Lett.* **54**, 2391 (1985).
27. B. Berkowitz, I. Balberg, *Transport in Porous Media* **9**, 275 (1992).
28. A. P. Friedman, N. A. Seaton, *Water Resources Res.* **34**, 1703 (1998).
29. A. Stogryn, G. J. Desargant, *IEEE Trans. Antennas Propagat.* **AP-33**, 523 (1985).

30. We are grateful for the support provided by the Division of Mathematical Sciences, the Arctic Natural Sciences Program, and the Division of Atmospheric Sciences at the US National Science Foundation (NSF). Adam Gully was supported by the NSF Research Experiences for Undergraduates (REU) Program and an NSF VIGRE graduate fellowship, Christian Sampson was supported by the NSF REU Program, and Joyce Lin was supported by an NSF VIGRE Postdoctoral Fellowship. We also thank the Australian Antarctic Division and the crew of the *Aurora Australis* for their help and support during the SIPEX Antarctic expedition.

Figure Captions

Figure 1: **(A)** A Wenner electrode array is configured to measure the vertical conductivity of Antarctic sea ice, by inserting the four probes into an extracted ice core. **(B)** A current I is injected into the core through the outer electrodes C1 and C2. The potential difference ΔV resulting from the current flow is measured by the inner electrodes P1 and P2. The ratio $\Delta V/I$ is the resistance R in ohms. Here the electrode spacing is $L = 10$ cm and $a = 10$ cm. **(C)** A cross-borehole array is frozen into Arctic sea ice. The DC resistivity profile was tomographically reconstructed in the volume enclosed by the electrode strings. One of the strings, with 10 cm separation of the plates, is shown in **(D)**.

Figure 2: The two dimensional square bond lattice below its percolation or connectivity threshold $p_c = 1/2$ in **(A)**, and above in **(B)**. Below p_c , there is no bulk transport, and above p_c the effective conductivity takes off with power law behavior, as shown in **(C)**. In **(D)** the effective resistivity diverges as p approaches p_c from the right, with a vertical asymptote at $p = p_c$. In **(E)** we display the vertical resistivity formation factor data from both the Antarctic (red squares) and Arctic (black diamonds) on a linear scale, along with the prediction from percolation theory. Both data and theory exhibit divergent behavior as ϕ approaches $\phi_c \approx 0.05$ from the right, with a vertical asymptote at $\phi = \phi_c$. **(F)** The Antarctic data is displayed on a logarithmic scale, and compared with $F = F_0(\phi - \phi_c)^2$, or $y = \log F = 2x + \log F_0$, $F_0 = 8.6$.

Figure 3: **(A)** Antarctic field data on the vertical formation factor $F = \sigma_v^*/\sigma_b$ is compared with the hierarchical model $F(\phi) = F_0\phi^3$. The prediction of percolation theory is also shown. **(B)** Comparison of Arctic fluid permeability data with the hierarchical model, along with percolation theory (12). In both figures percolation theory captures the trend of the data in the percolation regime more closely than Archie's law.

Figure 4: Cross-borehole tomographic reconstructions of the vertical resistivity formation factor for Arctic sea ice before (**A**) and after (**B**) melt pond formation. The evolution of resistivity structure seen here is consistent with warming of the ice, thus increasing the fluid permeability and facilitating the infiltration of meltwater into the upper layer of sea ice from the surface.

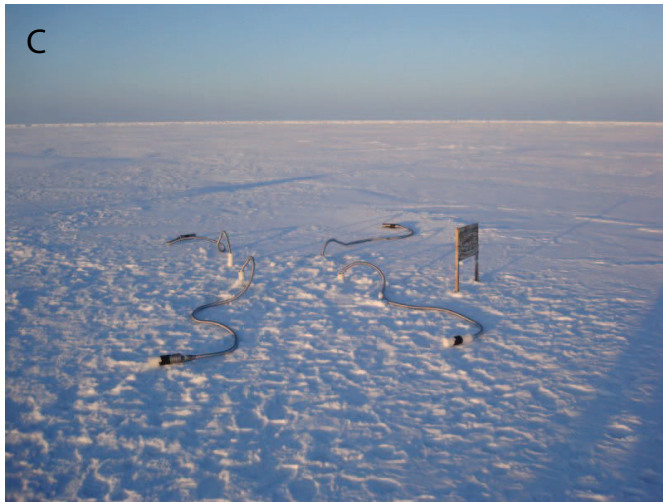
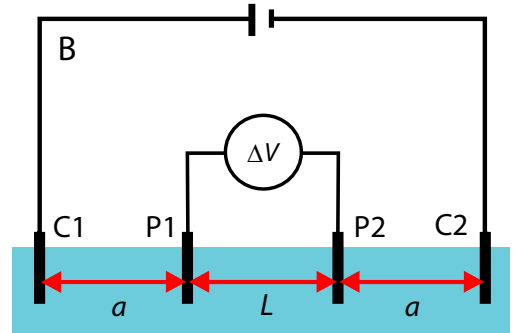
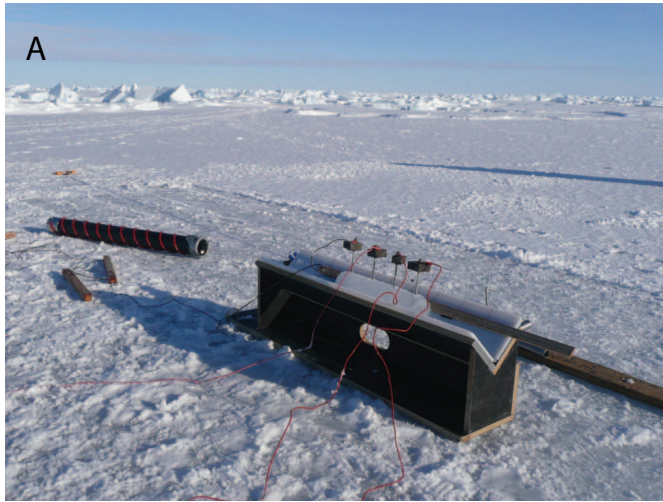


Figure 1:

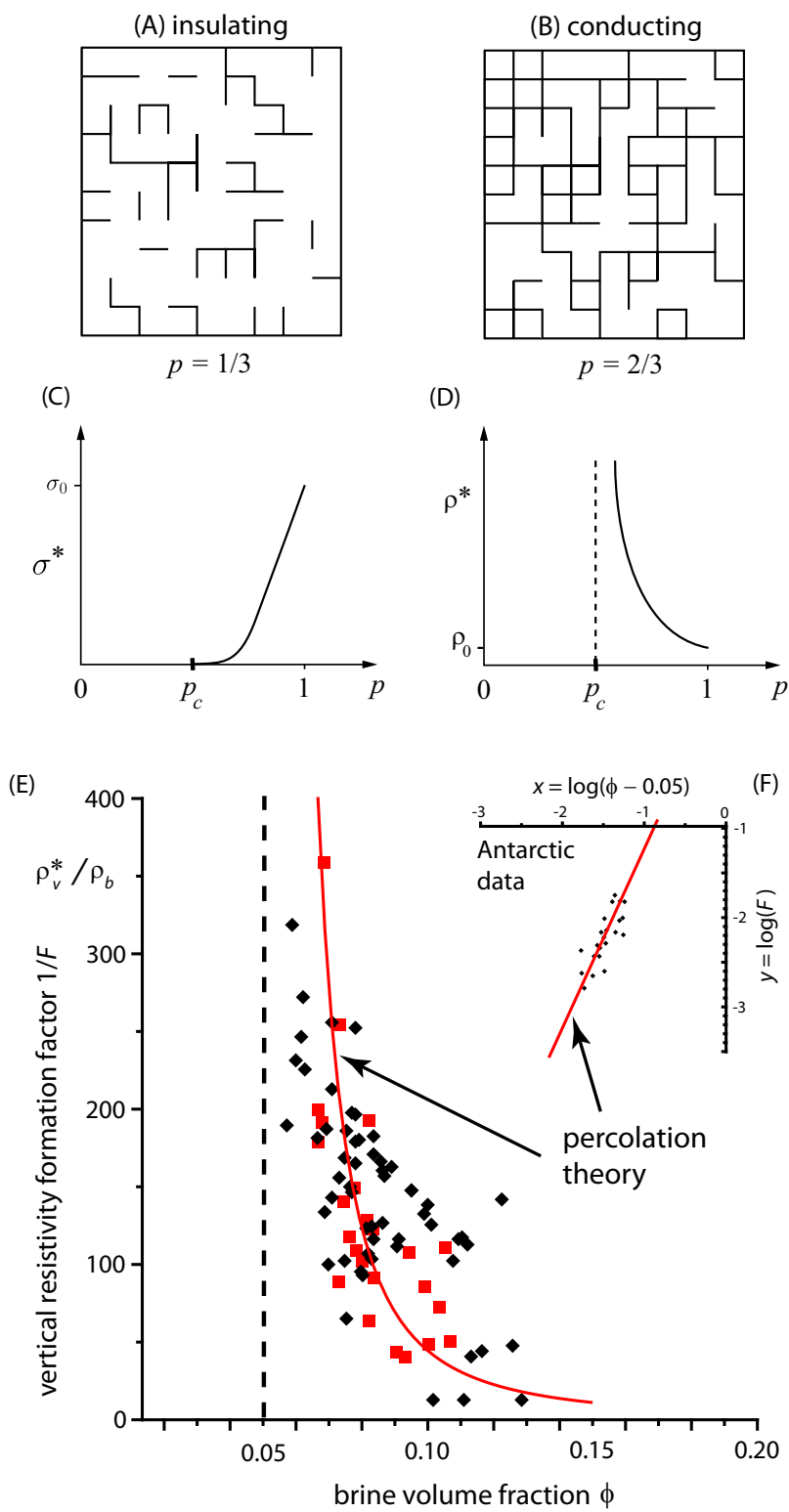


Figure 2:

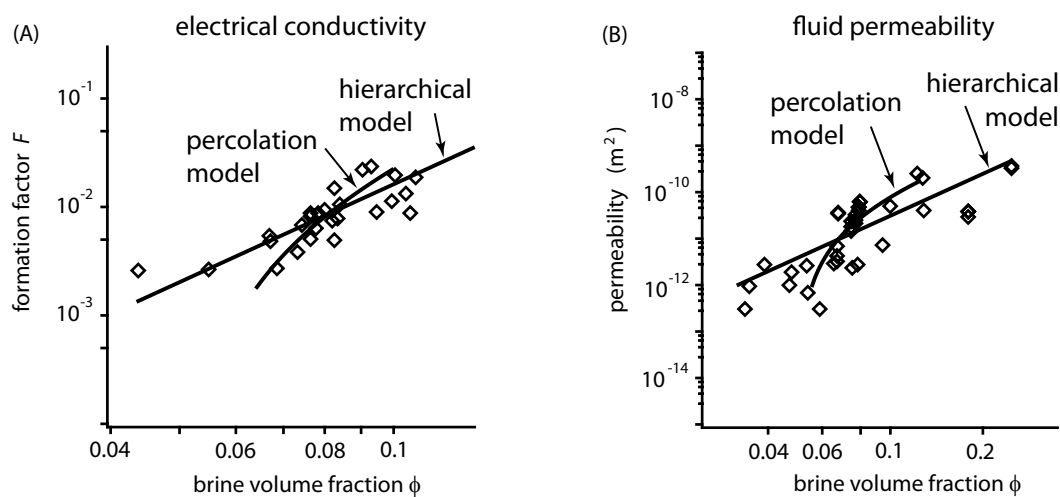


Figure 3:

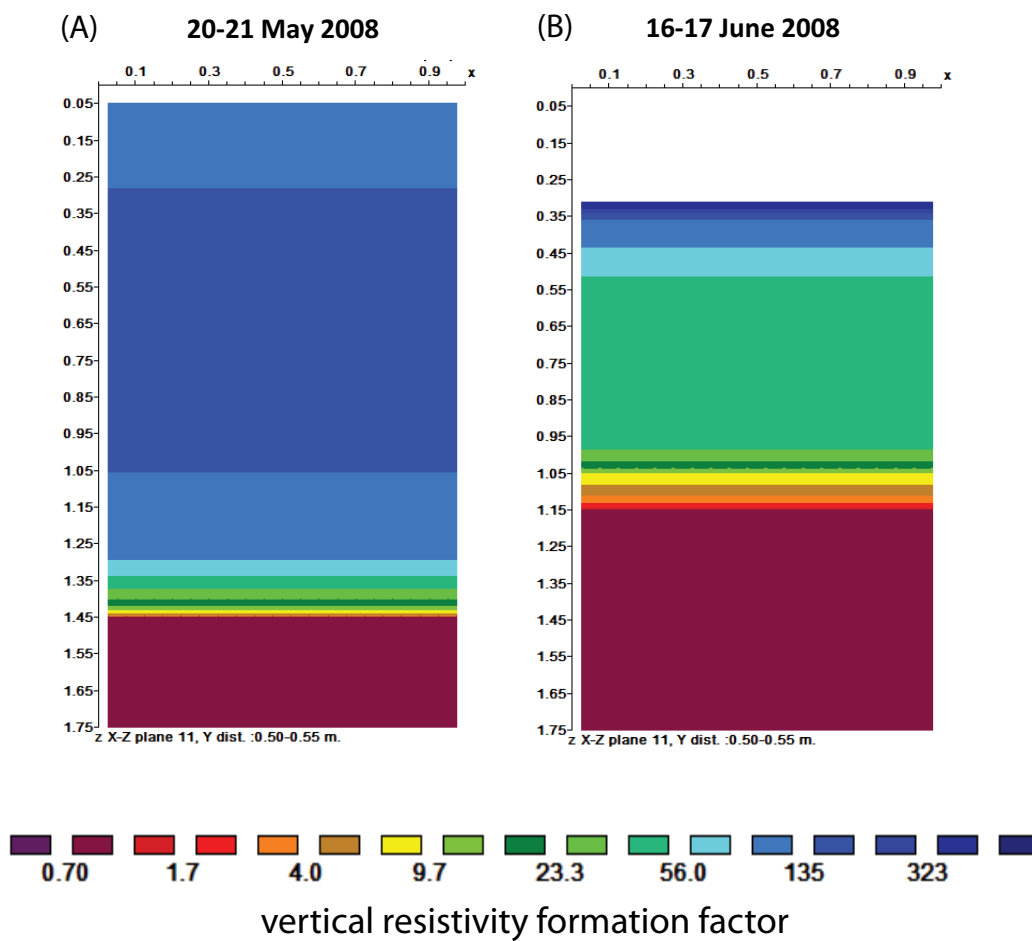


Figure 4: